Chemisorption-Induced Structural Changes and Transition from Chemisorption to Physisorption in Au6(CO)n-(n=4-9)

ARTICLE *in* THE JOURNAL OF PHYSICAL CHEMISTRY C · AUGUST 2008

Impact Factor: 4.77 · DOI: 10.1021/jp803161b

6 AUTHORS, INCLUDING:

Boggavarapu Kiran
McNeese State University
69 PUBLICATIONS **3,162** CITATIONS
SEE PROFILE

Jun Li
Tsinghua University
283 PUBLICATIONS **8,929** CITATIONS
SEE PROFILE

Lai-Sheng Wang
Brown University
434 PUBLICATIONS **18,876** CITATIONS
SEE PROFILE

Chemisorption-induced Structural Changes and Transition from Chemisorption to Physisorption in $Au_6(CO)_n^-$ ($n = 4-9$)

Hua-Jin Zhai,[†] Li-Li Pan,[‡] Bing Dai,[†] Boggavarapu Kiran,[†] Jun Li,*[,‡] and Lai-Sheng Wang*[,†]

Department of Chemistry & Key Laboratory of Organic Optoelectronics and Molecular Engineering of Ministry of Education, Tsinghua University, Beijing 100084, China, Department of Physics, Washington State University, 2710 University Drive, Richland, Washington 99354, and Chemical & Materials Sciences Division, Pacific Northwest National Laboratory, MS K8-88, P.O. Box 999, Richland, Washington 99352

Received: April 11, 2008; Revised Manuscript Received: May 16, 2008

The interactions of CO with gold clusters are essential to understanding the catalytic mechanisms of CO oxidation on supported gold nanoparticles. Here we report a photoelectron spectroscopy and theoretical study of CO adsorption on a well-defined Au_6^- cluster in $Au_6(CO)_n^-$ ($n = 4-9$). Previous studies have shown that the first three CO successively bind the three apex sites of the triangular Au_6^-. The current work reveals that the fourth CO induces a major structural change to create more apex sites to accommodate the additional CO. Definitive spectroscopic evidence is obtained for the chemisorption saturation at $Au_6(CO)_6^-$, in which Au_6 has rearranged to accommodate the six CO adsorbates. The photoelectron spectra of larger clusters from $Au_6(CO)_7^-$ to $Au_6(CO)_9^-$ are observed to be almost identical to that of $Au_6(CO)_6^-$, suggesting that the additional CO units are simply physisorbed onto the $Au_6(CO)_6^-$ core. Quasirelativistic density functional calculations are performed on both $Au_6(CO)_n$ and $Au_6(CO)_n^-$ ($n = 4-6$). The theoretical results are used to interpret the experimental observations and to provide insight into the nature of CO interactions with gold clusters. The Au_6 cluster is shown to be highly fluxional upon multiple CO adsorptions, stabilizing structures with more apex sites to accommodate the additional CO units. The CO-induced structural transformation is analogous to structural flexibility and mobility in heterogeneous catalysis. The observations of the propensity of CO toward apex sites and CO-induced structural changes in small gold clusters may be important for understanding the mechanisms of CO oxidation on supported gold nanoparticles.

1. Introduction

The extraordinary catalytic activities of nanosized gold particles,[1] in particular the oxidation of CO at low temperatures, have received considerable attention over the past few years.[2–10] However, the exact catalytic mechanisms for CO oxidation over supported gold nanoparticles are still not well understood.[11] The nature of CO and O_2 interactions with structurally well-defined Au clusters provides essential information to understand the mechanisms of the supported gold catalysts. Extensive research has been carried out along this direction, including size-selected cluster deposition studies[10] and gas-phase experimental[12–17] and theoretical[18–20] studies. A number of such studies have been devoted to the reactivity and chemisorption properties of size-selected Au clusters with CO in the gas phase. The chemisorption energies of CO on a wide range of Au_n^+ cluster cations for $n = 1-65$ have been reported, ranging from as large as 1.1 eV for smaller sizes to 0.65 eV for larger clusters.[15a] In a previous photoelectron spectroscopy (PES) study on CO-adsorbed Au cluster anions—$Au_m(CO)_n^-$ ($m = 2-5$; $n = 1-7$)[21]—we observed that the maximum number of chemisorbed CO on each Au cluster is equal to the number of low-coordination apex sites, and additional CO molecules are physisorbed. In the chemisorption regime, each CO is observed to have a profound effect on the electron binding energies of the $Au_m(CO)_n^-$ cluster complex, reducing the electron binding energies by as much as 0.6 eV per CO relative to the bare cluster, whereas physisorbed CO molecules have very little effect on the observed PES spectra.

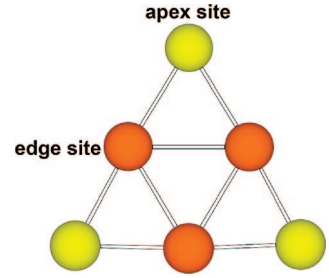

Figure 1. Schematic structure of the D_{3h} ground-state for Au_6^- and Au_6. The apex sites and edge sites are shown in different colors.

The gold hexamer is a unique cluster,[22] and both Au_6^- and Au_6 are known to possess a D_{3h} planar triangular structure with three apex sites and three edge sites, as shown in Figure 1. We have investigated previously CO-chemisorbed complexes of the gold hexamer—$Au_6(CO)_n^-$ ($n = 1-3$)—using PES and density functional theory (DFT) calculations[23] and found that, indeed, the first three CO units bind to the three apex sites successively without significantly perturbing the triangular structure of the parent cluster. A major surprise in that study is the observation that CO chemisorption appears to have little effect on the electron binding energies of the threshold PES band, but instead it significantly reduces the electron binding energies of the second PES band. In other words, the CO chemisorption has little effect on the LUMO of Au_6 but has a major effect on its HOMO. Through a detailed molecular orbital analysis, we found

* E-mail: (J.L.) junli@tsinghua.edu.cn, (L.S.W.) ls.wang@pnl.gov.
† Washington State University and Pacific Northwest National Laboratory.
‡ Tsinghua University.

10.1021/jp803161b CCC: $40.75
Published on Web 07/11/2008

that the LUMO of Au_6 changes from the outer triangle (the apex sites) to the inner triangle (the edge sites) in the CO-chemisorbed Au_6 complexes. Thus, the extra electron in Au_6^- is pushed from the outer triangle to the inner triangle by CO. The electron shuttling upon CO chemisorption between the spatially separated triangles was found to be responsible for the nearly constant electron affinities in $Au_6(CO)_n$ ($n = 0-3$).[23]

Because the gold hexamer has only three apex atoms (Figure 1), it is expected to be saturated with three chemisorbed CO molecules, and additional CO molecules should be physisorbed according to our previous finding that CO only prefers to chemisorb to apex sites.[21,23] However, a previous mass spectrometry study suggests that Au_6^- can chemisorb up to four CO molecules,[13a] whereas more recent studies suggest that both Au_6^+ and Au_6^- saturate with six CO molecules.[17] The questions thus arise: where do the extra CO molecules bind on the cluster, and what is the true chemisorption saturation limit of CO on the Au hexamer? The goal of the current work is to answer these questions. Because of the unique triangular structure of Au_6, which only features two types of atomic sites, a detailed study is feasible. Answers to these questions may provide further insight into the nature of CO interactions with Au clusters and the understanding of the cooperative chemisorption of CO and O_2 during the catalytic formation of CO_2.

We have obtained well-resolved PES spectra for $Au_6(CO)_n^-$ with $n = 4-9$, which represent the highest CO content ever reported for the gold hexamer. Our PES data indicate that a new isomer appears upon the adsorption of the fourth CO in $Au_6(CO)_4^-$, suggesting a possible CO-induced structural change. Chemisorption is observed up to $n = 6$, beyond which all additional CO molecules in $n = 7-9$ become physisorbed because their PES spectra are very similar to that for the $n = 6$ species. DFT calculations reveal that the triangular Au_6 framework undergoes major structural changes upon the adsorption of the fourth CO such that more apex sites are created to accommodate the additional CO. Upon further CO adsorption, three-dimensional (3D) structures become energetically competitive. In the lowest-lying 3D isomer of $Au_6(CO)_6^-$, all six Au atoms become apex sites to reach the chemisorption saturation limit. Beyond $Au_6(CO)_6^-$ no more CO molecules can be accommodated via chemisorption, and additional CO molecules are shown to be physisorbed. The CO-chemisorption-induced structural change in gold hexamer is interesting and is analogous to the well-known phenomenon of adsorbate-induced structural changes in heterogeneous catalysis.[24] The current work provides further confirmation for the concept that CO prefers apex sites when chemisorbed to Au clusters.

2. Experimental and Computational Methods

2.1. Photoelectron Spectroscopy. The experiment was carried out using a magnetic-bottle-type PES apparatus equipped with a laser vaporization supersonic cluster source, details of which were described elsewhere.[25] Briefly, the $Au_m(CO)_n^-$ cluster anions were produced by laser vaporization of a pure gold target in the presence of a helium carrier gas seeded with 2% CO. The $Au_m(CO)_n^-$ clusters with various compositions were generated and were separated using a time-of-flight mass spectrometer. We found that the Au and CO compositions in $Au_m(CO)_n^-$ can be tuned by controlling the residence time of the clusters in the nozzle. The longer the residence time, the more CO molecules are adsorbed in the $Au_m(CO)_n^-$ complexes. The long resident time also results in relatively cold clusters, enhancing the quality of the PES spectra.[26] We found that up to nine CO molecules can be adsorbed onto the gold hexamer in our source condition. We have previously studied the chemisorption behavior of the first three CO molecules,[23] and in the current work we focus on the high CO content species, $Au_6(CO)_n^-$ with $n = 4-9$. Each $Au_6(CO)_n^-$ complex with a given CO number was mass-selected and was decelerated before being photodetached. Two detachment photon energies were used in the current study: 266 nm (4.661 eV) and 193 nm (6.424 eV). Photoelectron spectra were calibrated using the known spectra of Au^- and Rh^-, and the energy resolution of the apparatus was $\Delta E_k/E_k \approx 2.5\%$, that is, ~25 meV for 1 eV electrons.

2.2. Density Functional Calculations. All DFT calculations were done using the NWChem program.[27] We employed the standard 6−31G* basis set[28] for oxygen and carbon and the Stuttgart 19-valence-electron relativistic energy-consistent pseudopotentials[29] and basis sets augmented with one f-type polarization functions ($\zeta_f = 0.498$) for gold.[30] We chose the B3LYP hybrid functional[31] to compute the electron binding energies because it worked well for the smaller $Au_6(CO)_n^-$ ($n = 1-3$) systems, as previously shown.[23] All calculations were spin-restricted for closed-shell molecules and spin-unrestricted for open-shell species. The first vertical detachment energy (VDE_1) was calculated using the ΔSCF energy difference between the neutral and the anion at the anion geometry. Higher VDE values were approximated using the generalized Koopman's theorem[32] by adding a constant correction term—$\delta E = E_1 - E_2 - \varepsilon_{HOMO}$—to the eigenvalues of the anion, where δE is the correction term, E_1 and E_2 are the total energies of the anion and neutral, respectively, in their ground states at the anion equilibrium geometry, and ε_{HOMO} corresponds to the Kohn−Sham eigenvalue of the HOMO of the anion. Density-of-states spectra were constructed by fitting the distribution of the VDE values with unit-area Gaussian functions of 0.04 eV full width at half-maximum (fwhm).

3. Experimental Results

The photoelectron spectra of $Au_6(CO)_n^-$ ($n = 4-9$) at 193 nm are shown in Figure 2, where the spectrum of $Au_6(CO)_3^-$ is also included for comparison. Our prior work on $Au_6(CO)_n^-$ ($n = 1-3$)[23] showed that chemisorption of the first three CO molecules has little effect on the first PES band (X), which has a nearly constant VDE of ~2.1 eV, identical to that for the bare Au_6^- cluster. In contrast, the first three CO molecules have profound effects on the second PES band (feature A in the $Au_6(CO)_3^-$ spectrum), decreasing the VDE of the A band by ~0.3−0.5 eV per CO and thus significantly reducing the X-A band gap.

A major spectral change was observed upon the fourth CO adsorption (Figure 2). The most dramatic change is the appearance of a new band in the lower binding energy range [X in the spectrum of $Au_6(CO)_4^-$]. The inset in Figure 2 shows a portion of the 266 nm spectrum of $Au_6(CO)_4^-$, resolving the new spectral feature more clearly. The new band (X) has a lower VDE of 1.75 eV, whereas the second component (X′) has a VDE (2.08 eV) similar to that of the X band in $Au_6(CO)_3^-$ (2.15 eV). The double-peak spectral pattern in the threshold region continues up to $Au_6(CO)_6^-$, except that the binding energy of the X band noticeably decreases and the relative intensities of the X versus X′ band increase from $n = 4$ to 6. These observations suggest that there are likely two isomers present in the spectra of $Au_6(CO)_n^-$ ($n = 4-6$), corresponding to the X and X′ spectral features. Hence, the fourth CO adsorption has induced a significant structural change to the Au_6 parent

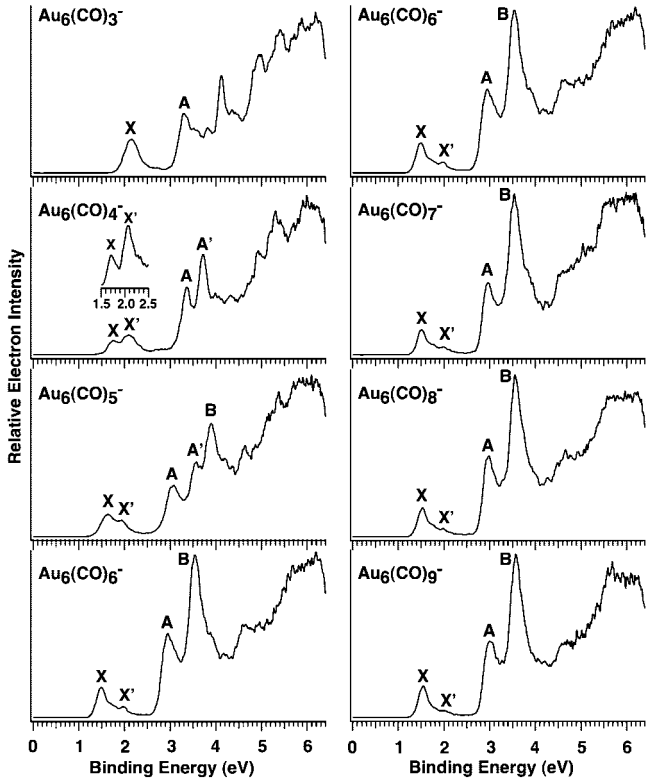

Figure 2. Photoelectron spectra of $Au_6(CO)_n^-$ ($n = 4-9$) at 193 nm (6.424 eV). Inset in $Au_6(CO)_4^-$ shows data at 266 nm (4.661 eV). The spectrum of $Au_6(CO)_3^-$ from ref 23 is shown for comparison.

TABLE 1: Observed Adiabatic and Vertical Detachment Energies (ADEs and VDEs) from the Photoelectron Spectra of $Au_6(CO)_n^-$ ($n = 4-9$)

		VDE (eV) [a,c]				
	ADE (eV) [a,b]	X	A	B	X′	A′
$Au_6(CO)_4^-$	1.63	1.75	3.36		2.08	3.72
$Au_6(CO)_5^-$	1.48	1.64	3.05	3.90	1.94	3.57
$Au_6(CO)_6^-$	1.42	1.49	2.95	3.54	1.98	
$Au_6(CO)_7^-$	1.45	1.51	2.96	3.54	1.99	
$Au_6(CO)_8^-$	1.47	1.53	2.98	3.56	1.99	
$Au_6(CO)_9^-$	1.48	1.54	3.01	3.58	2.01	

[a] Estimated experimental uncertainties: ± 0.05 eV. [b] Also represents electron affinities of the corresponding $Au_6(CO)_n$ neutral species. In all cases, the value corresponds to the low binding energy isomer, that is, the X band in Figure 2. [c] Spectral features X, A, and B are ascribed to one structural isomer, whereas X′ and A′ belong to another.

cluster. The spectrum of $Au_6(CO)_6^-$ is simpler and better resolved with three prominent bands (X, A, B), and the relative intensity of the X′ band becomes very weak, suggesting that there is only one dominating isomer for $Au_6(CO)_6^-$. An attempt was made to vary the relative isomer populations, but it was not successful because of the long source residence times needed to form the highly CO-adsorbed clusters, as mentioned above.

More interestingly, the spectra for $Au_6(CO)_n^-$ ($n = 7-9$) are all nearly identical to that of $Au_6(CO)_6^-$, each with the same three dominating bands (X, A, B) and the weak X′ band, as shown in the right column of Figure 2. But this similarity cannot be due to fragmentations of the larger clusters because these spectra are not exactly the same, and there is a slight shift of the ADEs from $n = 7$ to 9 (Table 1). These observations clearly show that $Au_6(CO)_6^-$ reaches the chemisorption saturation limit and that the additional CO molecules from $n = 7$ to 9 are weakly physisorbed to a $Au_6(CO)_6^-$ core, as will be discussed in Section 6.2. The electron detachment energies for all the resolved PES features are given in Table 1 for $Au_6(CO)_n^-$ ($n = 4-9$).

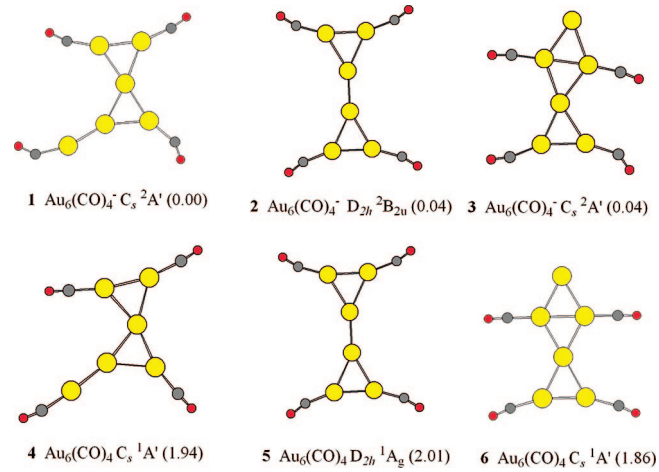

Figure 3. Optimized low-lying structures for $Au_6(CO)_4^-$ and $Au_6(CO)_4$. All relative energies (in eV) are referenced to the anion ground state.

4. Computational Results

The PES data suggest that once the three apex sites are used up additional isomers become competitive, consistent with our previous observation that the edge atoms do not seem to be good chemisorption sites.[21] Consequently, the triangular Au_6 parent needs to rearrange to create more apex sites to accommodate the additional CO molecules. We started our structural searches by placing the fourth CO to an edge site on $Au_6(CO)_3^-$, in which the first three CO molecules occupy the apex sites. We immediately found that the resulting structure is not a stable configuration. Following the imaginary vibrational mode, we located a stable structure **1** (Figure 3), which is due to the breaking of one Au−Au bond upon CO adsorption to an edge site. We further found that placing the fifth CO to the edge site also led to an unstable structure, that is, the triangular Au_6 is no longer stable when more than three CO molecules are chemisorbed. Consequently, we tested an extensive set of structures for $Au_6(CO)_n^-$ and $Au_6(CO)_n$ ($n = 4-6$), as collected in the Supporting Information (Figures S1−S3). The optimized low-lying structures (**1**−**18**) for $Au_6(CO)_n^-$ and $Au_6(CO)_n$ are presented in Figures 3-5 for $n = 4-6$, respectively. We also computed the ADE values and the first and second VDE values for the low-lying isomers (Table 2) to compare with the experimental results. The simulated PES spectra are shown in Figure 6 for the first three isomers of $Au_6(CO)_4^-$ and for the first two isomers each for $Au_6(CO)_5^-$ and $Au_6(CO)_6^-$. The computed CO chemisorption energies are given in Table 3, which also contains the energy differences (ΔE_{def}) between the deformed Au_6^- framework in the chemisorbed $Au_6(CO)_n^-$ complexes and the global minimum of the bare Au_6^-. This quantity will be helpful to understand the driving force for CO-induced structural changes. Because we are only concerned with the trend of the chemisorption energies, no corrections of the basis sets superposition errors were pursued.

4.1. $Au_6(CO)_4$ and $Au_6(CO)_4^-$. The optimized structures of the three low-lying isomers for $Au_6(CO)_4^-$ and $Au_6(CO)_4$ are shown in Figure 3. The anion ground state (**1**) is $^2A'$ with C_s symmetry, whereas the other two low-lying isomers (**2** and **3**) have $^2B_{2u}$ and $^2A'$ ground states with D_{2h} and C_s symmetries, respectively. These structures are energetically near-degenerate

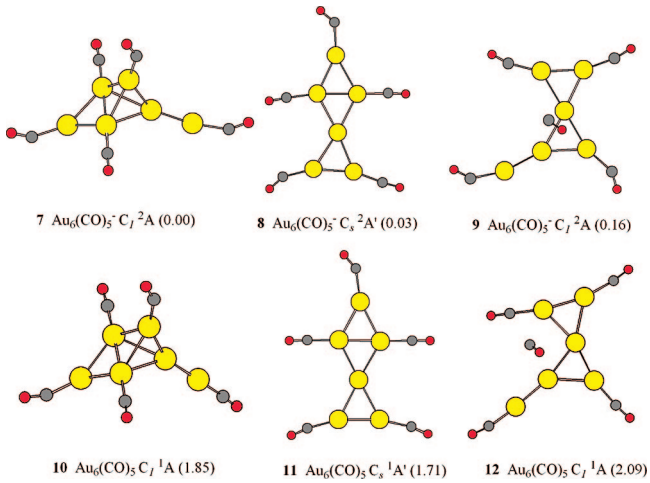

Figure 4. Optimized low-lying structures for $Au_6(CO)_5^-$ and $Au_6(CO)_5$. All relative energies (in eV) are referenced to the anion ground state.

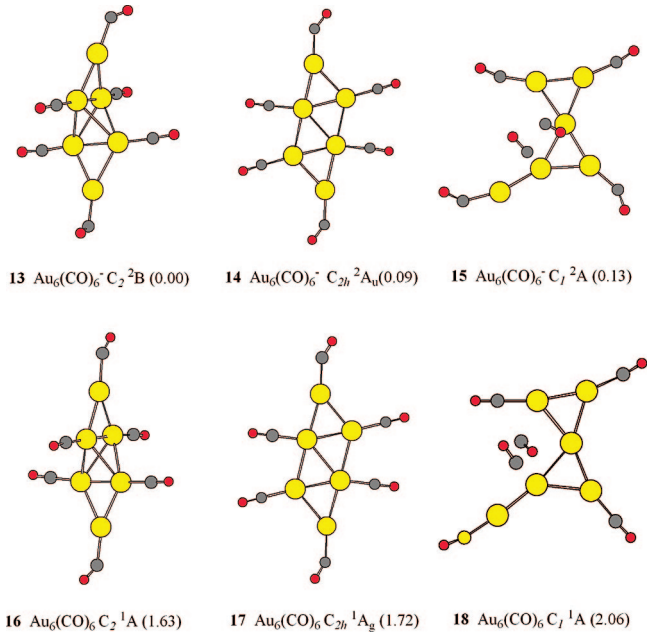

Figure 5. Optimized low-lying structures for $Au_6(CO)_6^-$ and $Au_6(CO)_6$. All relative energies (in eV) are referenced to the anion ground state.

TABLE 2: Theoretical Adiabatic and Vertical Detachment Energies of $Au_6(CO)_n^-$ (n = 4-6) (in eV)

	isomer	ADE	VDE_1[a]	VDE_2[a]
$Au_6(CO)_4^-$	**2**[b]	1.97	2.07	3.37
	1[c]	1.94	2.23	3.62
	3	1.82	2.08	3.49
$Au_6(CO)_5^-$	**8**[b]	1.68	1.88	3.21
	7[c]	1.85	2.15	3.43
	9	1.93	2.24	3.64
$Au_6(CO)_6^-$	**14**[b]	1.63	1.69	2.98
	13[c]	1.63	1.85	2.82
	15	1.93	2.24	3.68

[a] VDE_1 and VDE_2 denote the first and second VDE of $Au_6(CO)_n^-$, respectively. [b] Isomer assigned to the observed features X, A, and B in Figure 2. [c] Isomer assigned to the observed features X′ and A′ in Figure 2.

at the B3LYP level and cannot be differentiated without accurate account of the electron correlation effects (including dispersion effects) and the aurophilic interaction.[33] Both the total energies and VDE values of structures **2** and **3** are very close to each other at the current level of theory. Further computational studies using a high-level electron correlation method such as CCSD(T) and with full geometry optimizations are needed to determine the very small energy differences of these close-lying species, but those are computationally too challenging and are beyond the scope of the current work.

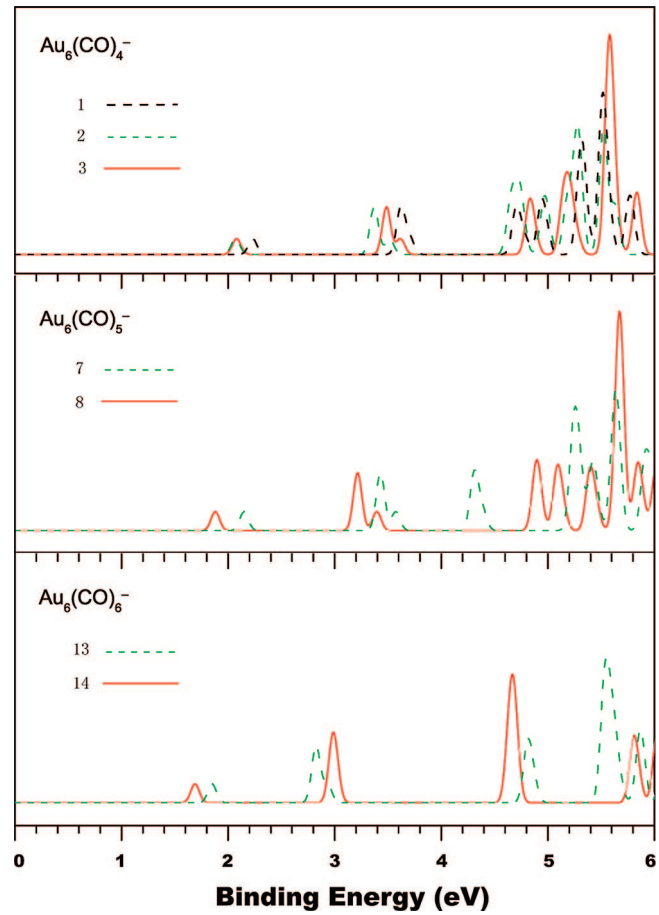

Figure 6. Simulated photoelectron spectra for the ground-state and low-lying structures of $Au_6(CO)_n^-$ (n = 4−6). The labels are the same as in Figures 3–5. The spectra were constructed by fitting the distribution of the calculated VDE values with unit-area Gaussian functions of 0.04 eV fwhm.

TABLE 3: Computed Average Chemisorption Energy per CO (in eV) in $Au_6(CO)_n^-$ and $Au_6(CO)_n$ (n = 4-6)

	anion[a]	neutral[a]	ΔE_{def}[b]
$Au_6(CO)_4$	0.75 (**1**)	0.88 (**4**)	0.23
	0.93 (**2**)	0.89 (**5**)	1.02
	0.88 (**3**)	0.99 (**6**)	0.94
$Au_6(CO)_5$	0.84 (**7**)	0.88 (**10**)	0.55
	0.81 (**8**)	0.93 (**11**)	0.94
$Au_6(CO)_6$	0.82 (**13**)	0.93 (**16**)	1.62
	0.85 (**14**)	0.81 (**17**)	0.23

[a] The numbers in the brackets are the serial numbers of the structures as shown in Figures 3–5. [b] ΔE_{def} denotes the energy difference between the deformed Au_6^- framework in chemisorbed $Au_6(CO)_n^-$ complexes and the undistorted bare Au_6^- (D_{3h}) (Figure 1).

The three corresponding isomers for the $Au_6(CO)_4$ neutral (**4**, **5**, and **6**) are $^1A'$ (C_s), ^1A_g (D_{2h}), and $^1A'$ (C_s), respectively. Note that all of the four CO molecules occupy apex sites in the low-lying isomers of $Au_6(CO)_4^-$ and $Au_6(CO)_4$ with substantial chemisorption energies (Table 3), consistent with our previous observations that CO prefers to chemisorb to apex sites.[21,23]

4.2. $Au_6(CO)_5$ and $Au_6(CO)_5^-$. The lowest energy isomer for the $n = 5$ species becomes three dimensional (3D) (**7** in Figure 4). Among the three low-lying isomers of $Au_6(CO)_4^-$, only isomer **3** has an open apex site, which indeed becomes a low-lying isomer for $Au_6(CO)_5^-$ (**8**). This isomer is only 0.03 eV higher than the 3D structure **7**, and they should be considered degenerate at the current level of theory. These two structures both possess five apex sites for CO chemisorption with high CO binding energies (Table 3). Structure **9** is based on structure **1** of $Au_6(CO)_4^-$ with the additional CO physisorbed to a nonapex Au atom above the plane of Au_6. This physisorbed structure is only 0.16 eV higher than structure **7**. In the neutral, structure **11**, which corresponds to the anion **8**, becomes the most stable structure. The 3D structure **10** is 0.14 eV higher, whereas the physisorbed structure **12** is 0.38 eV higher.

4.3. $Au_6(CO)_6$ and $Au_6(CO)_6^-$. The lowest-energy isomer of $Au_6(CO)_6^-$ **13** (Figure 5) is also a 3D structure, in which the Au_6 framework is rearranged to a bibridged tetrahedron. In this structure, all six Au atoms become apex sites. A 2D structure (**14**) is only 0.09 eV higher, even though it only possesses four apex sites. A structure (**15**) with two physisorbed CO molecules onto the lowest-energy structure of $Au_6(CO)_4^-$ (**1**) is only 0.13 eV higher in energy. Interestingly, the structure with six CO molecules chemisorbed to the triangular Au_6^- is indeed a minimum (**59**, Figure S3), but it is 0.34 eV higher than the ground-state isomer **13** (i.e., **56** in Figure S3). This structure has been proposed previously,[20b] but it is clearly not energetically competitive because of the three unfavorable edge sites for CO chemisorption. Note that isomer **14** (i.e., **57** in Figure S3) with only two edge sites is much more energetically favored. The low-lying isomers for neutral $Au_6(CO)_6$ (**16**−**18**) exhibit similar energetic orders as the anions. Again, without high-level electron correlation calculations, the stabilities of the isomers of neutral $Au_6(CO)_6$ and anionic $Au_6(CO)_6^-$ can hardly be determined by DFT calculations alone because of the small energy differences among the different isomers.

5. Comparison between Experiment and Theory

Both the experimental and computational results for $Au_6(CO)_n^-$ ($n = 4-6$) demonstrate the complexity of these systems. The competition between various closely lying isomers imposes considerable computational challenges due to the complicated chemical and physical interactions between Au−Au and Au−CO. As a result of the self-interaction error and lack of dispersion interaction, DFT methods such as B3LYP might have a large error bar in calculating the total energies of isomers with significantly different structures, such as 2D versus 3D structures. In the following we qualitatively interpret the experimental data on the basis of the DFT calculations. We focus on the qualitative trend rather than the quantitative ADE and VDE values, which we consider as a reliable criterion for the spectral assignments.

5.1. $Au_6(CO)_4^-$. The simulated spectra for the three low-lying structures of $Au_6(CO)_4^-$ (**1**−**3**) are shown in Figure 6 (top panel), which are in reasonable agreement with the experimental spectrum. Isomer **1** displays higher electron binding energies and is assigned to be responsible for the observed X′ and A′ bands (Figure 2). Both isomers **2** and **3** give nearly identical VDE values for the ground-state transition (Table 2), but their second VDE values are different; the second VDE of isomer **3** is higher than that of isomer **2**. Comparison between the simulated spectra and the experimental spectrum suggests that the A band is most likely due to contribution from isomer **2** (the green curve in Figure 6) because if isomer **3** (red curve in Figure 6) were to make significant contributions then the A and A′ bands could not have been well resolved. Thus, we tentatively assign the second isomer present in the experiment as structure **2**. The relative spectral intensities suggest that isomer **1** is more abundant, which is reasonable because this isomer can be viewed as a distortion from CO chemisorption to an edge site of $Au_6(CO)_3^-$, whereas isomer **2** involves much more extensive rearrangement from the triangular Au_6^- framework.

5.2. $Au_6(CO)_5^-$. Simulated spectra for the two lowest energy structures of $Au_6(CO)_5^-$ are shown in Figure 6 (middle panel). Isomer **8** shows lower electron binding energies (Table 2 and red curve in Figure 6) and is tentatively assigned to be responsible for the observed X and A bands in the PES spectrum of $Au_6(CO)_5^-$ (Figure 2), whereas isomer **7** possesses slightly higher binding energies (green curve in Figure 6, middle panel) and is assigned to be responsible for the X′ and A′ bands. The calculated VDE values for the first two detachment channels for these isomers are in reasonable agreement with the observed spectral features, although higher binding energy features, in particular band B, are not well reproduced. The relative intensities of the X and X′ bands suggest that isomer **8** is more dominant, which is reasonable because this isomer is planar and involves much less rearrangement from the triangular Au_6^- compared to the 3D Au_6^- framework of isomer **7**. Both of these isomers possess five apex sites, which are fully occupied by the five CO molecules. A previous IR study on $Au_m(CO)_n^+$ cations suggests a possible saturation of five chemisorbed CO molecules onto Au_6^+.[17a] Either isomer **7** or **8** might be a reasonable candidate for the observed $Au_6(CO)_5^+$ complex.

5.3. $Au_6(CO)_6^-$. The PES spectrum of $Au_6(CO)_6^-$ (Figure 2) indicates one dominant isomers with low electron binding energies. A weak isomer is present (X′), which has a slightly higher electron binding energy. The simulated spectra for the two lowest energy isomers of $Au_6(CO)_6^-$ are shown in Figure 6 (bottom panel). Clearly, the first and second main PES bands (X and A, Figure 2) are in good agreement with the simulated spectrum of isomer **14**, although the strong B band (VDE = 3.54 eV) observed experimentally does not seem to have a corresponding simulated peak. The third calculated detachment transition for isomer **14** occurs at a VDE of ∼4.7 eV. It is likely that spin−orbit coupling effects, which are not considered in these calculations, could shift this band calculated at the scalar relativistic level. We tentatively assign the minor isomer to be from isomer **13**. Again, the dominance of isomer **14** is reasonable because it involves only a minor in-plane rearrangement from the triangular Au_6^-, whereas major structural rearrangements are involved to form the 3D Au_6^- framework of isomer **13**.

6. Discussion

6.1. CO Chemisorption-Induced Structural Changes in $Au_6(CO)_n^-$ ($n = 4-6$). Both experimental and computational results show that successive adsorption of CO on Au_6^- can distort the Au cluster framework beyond $n = 3$. The spectral change from $Au_6(CO)_3^-$ to $Au_6(CO)_4^-$ (Figure 2) suggests that new isomers appear upon adsorption of the fourth CO, which is confirmed by the theoretical results. The consequences of the structural distortions are to create more apex sites to accommodate the additional CO molecules. This derives from the competition between the relatively weak Au−Au bonding and the optimal Au−CO bonding. The current result confirms our previous observation that the apex sites are the preferred CO chemisorption sites on small Au clusters.[21,23] The facile structural distortion is also assisted by the structural fluxionality of the triangular Au_6 framework, that is, the relatively weak

Au−Au bonding and the softness of the vibrational modes of Au clusters. CO chemisorption was previously observed to induce structural changes in small Ni clusters.[34] More interestingly, the current result is similar to a previous experiment of C_2H_4 chemisorption on small silver clusters,[35] where Ag_5^+ was observed to undergo major structural changes upon the third C_2H_4 adsorption to allow accommodation of more ligands. Structural flexibility and mobility have been known to be critical in heterogeneous catalysis.[24] These may also be important features for catalysis on gold nanoclusters.

To quantify the driving force for the structural transformations upon CO adsorption in $Au_6(CO)_n^-$ ($n = 4-6$), we have computed the CO chemisorption energies in the various low-lying isomers for both the anions and the neutral chemisorbed complexes, as given in Table 3. Also shown in Table 3 are the energy differences between the corresponding Au_6^- framework in the chemisorbed complexes and the bare Au_6^- triangle structure (the global minimum of Au_6^-, Figure 1). We find that the CO chemisorption energies are quite large in all the different isomers, averaging 0.8−0.9 eV per CO in the anions.[36] The neutral complexes display only slightly larger chemisorption energies. We note that the CO binding energy to the Au_6^+ cation has been measured as ~1.0 eV,[15a] quite comparable to our calculated values for the neutral and anion. As shown in Table 3, the energy difference between the distorted Au framework and the ground-state triangular structure range from 0.23 (**1**) to 1.62 eV (**13**), which are not too large and can be readily compensated by the enhanced Au−CO bonding.

6.2. Transition from Chemisorption to Physisorption in $Au_6(CO)_n^-$ ($n = 7-9$). Previous mass spectrometric and IR studies indicated the saturation coverage of CO to be either 4 or 6 for Au_6^- and 5 or 6 for Au_6^+.[13a,17] The current PES data reveal definite spectroscopic evidence that CO chemisorption on Au_6^- saturates at $n = 6$, rather than at $n = 4$. Additional CO molecules beyond the saturation limit have very little effect on the PES spectra (Figure 2), and a transition from chemisorption to physisorption takes place. Similar transitions from chemisorption to physisorption were also observed in our previous work on smaller clusters, $Au_m(CO)_n^-$ ($m = 2-5$; $n = 1-7$),[21] as well as in C_2H_4 adsorption on small Ag_n^+ clusters.[35] Clearly, PES is quite sensitive to the nature of the adsorbate−cluster interactions and provides a spectroscopic means to distinguish between chemisorption versus physisorption.

As an example, we simulated the VDE spectra of structure **1** of $Au_6(CO)_4^-$ (Figure 3) and its physisorbed species by one and two CO molecules, which have been located in our DFT calculations: **9** for $Au_6(CO)_5^-$ (Figure 4) and **15** for $Au_6(CO)_6^-$ (Figure 5). As shown in Figure 7, the simulated spectra of the three complexes are virtually identical, indeed confirming that physisorption of CO does not affect in any significant way the electronic and geometric structures of the chemisorbed core complex. In the $Au_6(CO)_n^-$ ($n = 7-9$) complexes, the CO molecules beyond the saturation limit are likely physisorbed to isomer **14** of $Au_6(CO)_6^-$ (Figure 5) above or below the plane of the Au_6 framework. It is important to note that although CO chemisorption induces a significant red-shift to the electron binding energies, the physisorbed CO induces a very small blue-shift (see Figure 2 and Table 1).[21] The red-shift is due to the charge donation from CO to the Au clusters in the chemisorption regime, whereas the small blue-shift in the physisorption regime reflects the dispersion interactions between the additional CO molecules and the chemisorbed core. Interestingly, the onset of spectral red-shift in the $Au_6(CO)_n^-$ ($n = 0-9$) series and structural transition at $Au_6(CO)_4^-$ coincide with a previous observation of pronounced cooperative coadsorption of CO and O_2 in the $Au_6(CO)_4O_2^-$ complex.[13b] Clearly, the CO chemisorption-induced electronic and structural changes in $Au_6(CO)_4^-$ promote the binding of O_2.

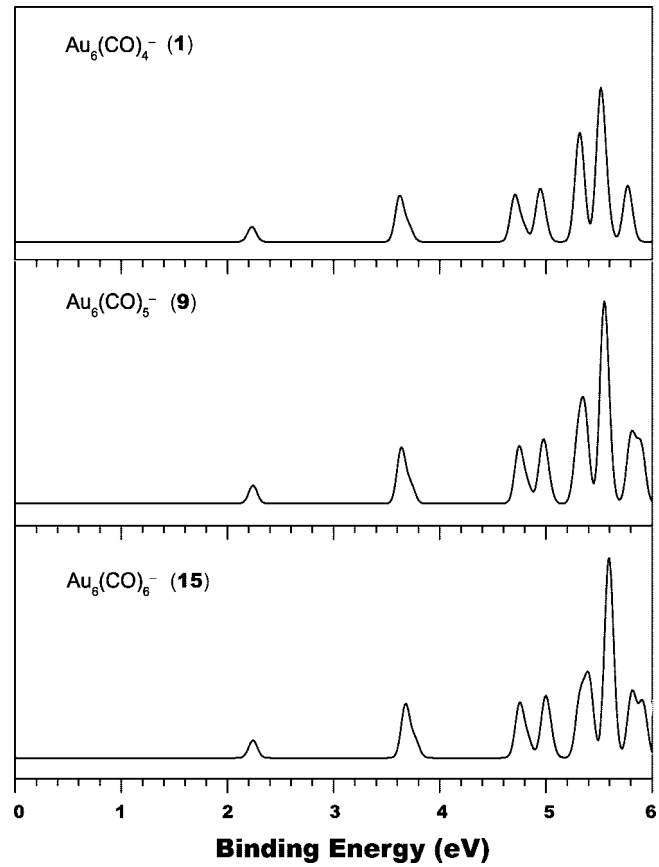

Figure 7. Comparison of the simulated photoelectron spectrum of $Au_6(CO)_4^-$ (**1**) with those physisorbed by one (**9**) and two CO molecules (**15**). The spectra were constructed by fitting the distribution of calculated VDEs with unit-area Gaussian functions of 0.04 eV fwhm.

6.3. Why Does CO Prefer the Apex Sites in Au Clusters? We have thus far shown that CO prefers to bind the apex sites rather than the edge sites of small gold clusters.[21,23] On the Au_{20} pyramid[37] we found that CO adsorption is about 6 times stronger for an apex site than for a face-center site. Interestingly, the D_{3h} Au_6 is a fragment of one of the Au_{20} surfaces, and the edge sites in Au_6 also correspond to the edge sites in Au_{20}.[37] To understand the nature of why CO prefers the apex sites to the edge sites in Au_6^-, we performed further DFT calculations to determine the binding energy curves of CO approaching the two types of sites in Au_6^-. The calculations were performed on the two low-lying $^2A_1$ and $^2B_2$ states of $Au_6(CO)^-$ with Au−CO distances of 1−6 Å.[38] Figure 8 shows the binding energy curves of the $^2A_1$ state for the edge site and the $^2B_2$ state for the apex site of $Au_6(CO)^-$, and the optimized geometries of these two states together with that of Au_6^- are shown in Figure 9. The binding energy curves for the other two states ($^2A_1$ for the apex site and $^2B_2$ state for the edge site) are not shown because the calculations indicate that for the edge site $^2A_1$ is more stable than $^2B_2$ by 0.47 eV, whereas for the apex site $^2B_2$ is more stable than $^2A_1$ by 0.44 eV. Figure 8 shows that CO can bind either to the apex or to the edge site of Au_6^- with a Au−CO distance around 1.9 Å (Figure 9).

However, significant energetic and bonding differences exist between the two types of adsorption sites. As shown below,

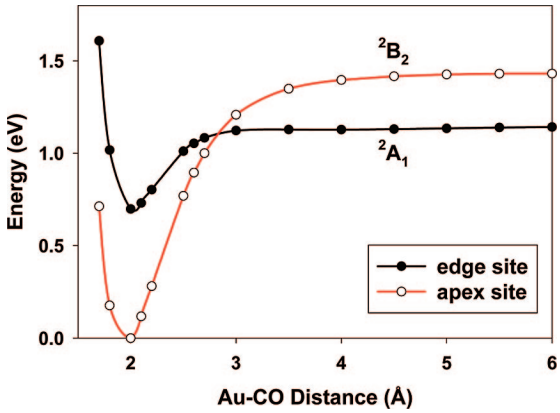

Figure 8. The binding energy curves for adsorption of a CO molecule to an apex site ($^2B_2$, red curve) and to an edge site ($^2A_1$, black curve) of the Au_6^- cluster (see Figure 9).

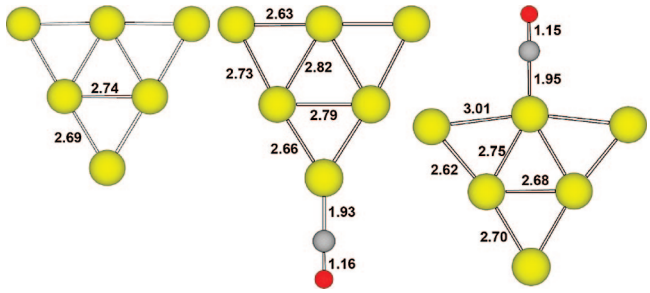

Figure 9. Optimized geometries of Au_6^- (D_{3h}), $Au_6(CO)^-$ (apex, $^2B_2$, C_{2v}), and $Au_6(CO)^-$ (edge, $^2A_1$, C_{2v}). The bond lengths listed are in Angstroms.

CO adsorption to the apex site involves direct chemical interaction between CO and Au atoms. On the other hand, CO adsorption to the edge site will encounter steric repulsion from the two neighboring apex atoms. As shown in Figure 9, upon adsorption of CO to the apex site there is no significant geometry change in the Au_6 framework, whereas when CO is adsorbed at the edge sites the two neighboring atoms are considerably pushed out by about 0.3 Å. Consequently, at the potential energy minima, the CO binding is ~0.7 eV more stable for the apex sites than for the edge sites at PW91 level[38] because the adsorption of CO on the edge sites deforms and weakens bonding within the Au_6 framework. As shown in Figure 9, CO is markedly activated at the apex site, and the optimized C−O distance is 0.01 Å longer for the apex sites than for the edge sites.

These structural and energetic differences for adsorptions of CO on the apex and edge sites of Au_6^- can be understood from orbital and bonding analyses (Figure 10). When Au atoms form the D_{3h} Au_6 framework, the Au 6s orbitals form a set of bonding ($2a_1' + 6e'$) and nearly degenerate antibonding ($6a_1' + 8e'$) orbitals, where $6a_1'$ is mainly from the outer triangle (apex sites) and 8e′ is from the inner triangle (edge sites) (also see Figure 6 in ref 23). When CO approaches Au_6^-, there are significant closed-shell repulsions between the occupied Au_6^- orbitals and the CO 5σ donor orbital (and the 4σ orbital to a less extent), leading to the destabilization of the former and stabilization of the latter. Upon adsorption of CO at an apex site, the net interactions include σ-bonding between the Au_6^- $6a_1'$ orbital and the CO 5σ donor orbital, as well as weak π back-donation bonding between the framework 8e′-based orbitals and the CO 2π orbitals, leading to the formation of a $^2B_2$ ground state (see Figure 6 in ref 23).

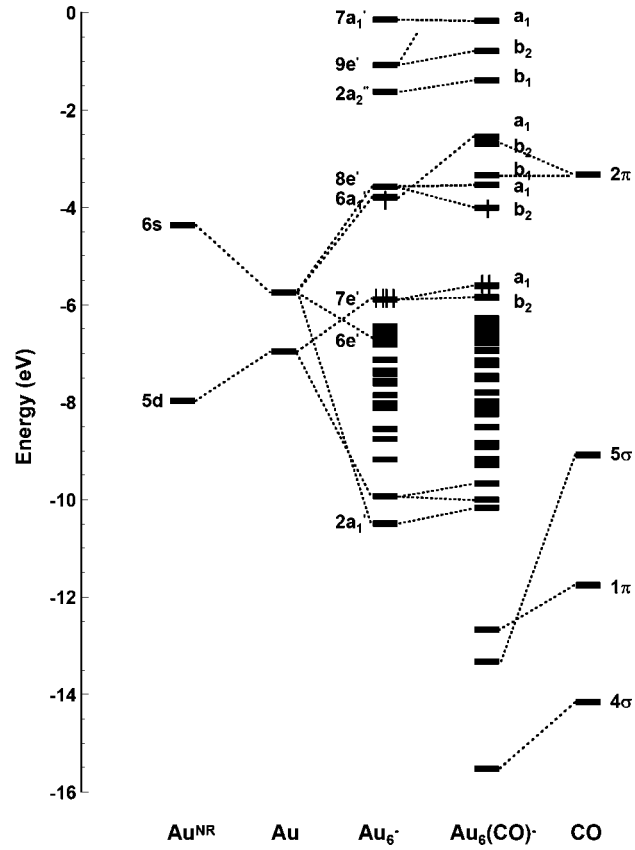

Figure 10. Orbital interactions between an apex site of Au_6^- and CO in $Au_6(CO)^-$. The Au^{NR} energy levels are from nonrelativistic calculations, and all the other energy levels are from scalar relativistic calculations.

In contrast, when CO approaches the edge site, the apex-site based $6a_1'$ orbital of Au_6^- is singly occupied, forming a $^2A_1$ ground state. σ-Bonding can occur between the Au_6^- 8e′ and the CO 5σ orbitals, but there is no π back-donation from Au_6^- to CO. Our PW91 calculations indicate that for the apex site adsorption, there is 23% CO 2π character in the singly occupied b_2 orbital (Figure 10), whereas for the edge site adsorption there is no CO 2π character in the singly occupied a_1 orbital due to symmetry mismatch. Furthermore, the singly occupied $6a_1'$ orbital of Au_6^- is repulsive with the CO 5σ orbital, resulting in the elongation of the Au−Au distance between the edge site and its two neighboring apex sites. In a nonplanar Au cluster, CO adsorption to an edge site is expected to experience even more repulsion from the neighboring atoms, as is the case in the Au_{20}−CO complexes.[37] On a flat surface, the CO binding is known to be even weaker, such as on bulk gold or on the face-center site in Au_{20}. Isomer **9** for $Au_6(CO)_5^-$ (Figure 4) and isomer **15** for $Au_6(CO)_6^-$ (Figure 5) also clearly show that CO only physisorbs onto the plane of the Au_6 substrate. The clear preference of CO to apex sites on small gold clusters may be important for understanding CO chemisorption on the surface of gold nanoparticles.

7. Conclusions

We report a combined experimental and theoretical study of highly CO-adsorbed gold clusters, $Au_6(CO)_n^-$ ($n = 4-9$). Well-resolved photoelectron spectra were obtained, revealing evidence for structural changes induced by the fourth CO adsorption and for the coexistence of multiple isomers. A clear chemisorption saturation at six CO molecules was observed; the photoelectron

spectra of $Au_6(CO)_n^-$ ($n = 7-9$) were observed to be nearly identical to that of $Au_6(CO)_6^-$, indicating that the additional CO molecules are weakly physisorbed to a $Au_6(CO)_6^-$ core. Extensive density functional calculations were carried out for both $Au_6(CO)_n$ and $Au_6(CO)_n^-$ ($n = 4-6$) and were used to interpret the observed photoelectron spectra and to understand the nature of CO−Au_6 interactions. The calculations show that the fourth CO induced a major structural change to the triangular Au_6 substrate to create additional apex sites for further CO chemisorption. The current results confirm previous studies that CO prefers to bind to apex sites on small gold clusters. Detailed theoretical calculations were presented to understand the preference of apex versus edge site by CO in $Au_6(CO)^-$. The preference of CO adsorption to apex sites may be important to understand the mechanisms of CO oxidation on Au nanoparticle. The structural transformations of the Au_6 substrate upon CO chemisorption are analogous to adsorbate-induced structural flexibility and mobility in heterogeneous catalysis[24] and could also play an important role in the catalysis of gold nanoparticles.

Acknowledgment. This work was supported by the National Science Foundation (CHE-0349426) and performed at EMSL, a national scientific user facility sponsored by the Department of Energy's Office of Biological and Environmental Research and located at the Pacific Northwest National Laboratory, operated for DOE by Battelle. The theoretical work was supported by NKBRSF (2006CB 932305, 2007CB815200) and NNSFC (20525104) in China. The calculations were performed using a HP Itanium2 cluster at Tsinghua National Laboratory for Information Science and Technology and with supercomputers at the EMSL Molecular Science Computing Facility.

Supporting Information Available: Alternative optimized structures for $Au_6(CO)_n^-$ and $Au_6(CO)_n$ ($n = 4-6$) along with their relative energies (Figures S1−S3) and the complete ref 27. This material is available free of charge via the Internet at http://pubs.acs.org.

References and Notes

(1) (a) Haruta, M. *Catal. Today* **1997**, *36*, 153. (b) Haruta, M. *Chem. Rec.* **2003**, *3*, 75.

(2) (a) Bond, G. C.; Thompson, D. T. *Catal. Rev. Sci. Eng.* **1999**, *41*, 319. (b) Meyer, R.; Lemire, C.; Shaikhutdinov, S. K.; Freund, H.-J. *Gold Bull.* **2004**, *37*, 72.

(3) (a) Valden, M.; Lai, X.; Goodman, D. W. *Science* **1998**, *281*, 1647. (b) Chen, M. S.; Goodman, D. W. *Science* **2004**, *306*, 252. (c) Chen, M. S.; Kumar, D.; Yi, C. W.; Goodman, D. W. *Science* **2005**, *310*, 291.

(4) (a) Kim, T. S.; Stiehl, J. D.; Reeves, C. T.; Meyer, R. J.; Mullins, C. B. *J. Am. Chem. Soc.* **2003**, *125*, 2018. (b) Stiehl, J. D.; Kim, T. S.; McClure, S. M.; Mullins, C. B. *J. Am. Chem. Soc.* **2004**, *126*, 1606.

(5) (a) Guzman, J.; Gates, B. C. *J. Am. Chem. Soc.* **2004**, *126*, 2672. (b) Date, M.; Okumura, M.; Tsubota, S.; Haruta, M. *Angew. Chem., Int. Ed.* **2004**, *43*, 2129. (c) Lemire, C.; Meyer, R.; Shaikhutdinov, S.; Freund, H. J. *Angew. Chem., Int. Ed.* **2004**, *43*, 118. (d) Deng, X.; Min, B. K.; Guloy, A.; Friend, C. M. *J. Am. Chem. Soc.* **2005**, *127*, 9267.

(6) (a) Hughes, M. D.; Xu, Y. J.; Jenkins, P.; McMorn, P.; Landon, P.; Enache, D. I.; Carley, A. F.; Attard, G. A.; Hutchings, G. J.; King, F.; Stitt, E. H.; Johnston, P.; Griffin, K.; Kiely, C. J. *Nature* **2005**, *437*, 1132. (b) Enache, D. I.; Edwards, J. K.; Landon, P.; Solsona-Espriu, B.; Carley, A. F.; Herzing, A. A.; Watanabe, M.; Kiely, C. J.; Knight, D. W.; Hutchings, G. J. *Science* **2006**, *311*, 362.

(7) (a) Sterrer, M.; Yulikov, M.; Risse, T.; Freund, H.-J.; Carrasco, J.; Illas, F.; Di Valentin, C.; Giordano, L.; Pacchioni, G. *Angew. Chem., Int. Ed.* **2006**, *45*, 2633. (b) Sterrer, M.; Yulikov, M.; Fischbach, E.; Heyde, M.; Rust, H. P.; Pacchioni, G.; Risse, T.; Freund, H.-J. *Angew. Chem., Int. Ed.* **2006**, *45*, 2630. (c) Matthey, D.; Wang, J. G.; Wendt, S.; Matthiesen, J.; Schaub, R.; Lægsgaard, E.; Hammer, B.; Besenbacher, F. *Science* **2007**, *315*, 1692.

(8) (a) Liu, Z. P.; Hu, P.; Alavi, A. *J. Am. Chem. Soc.* **2002**, *124*, 14770. (b) Liu, Z. P.; Gong, X. Q.; Kohanoff, J.; Sanchez, C.; Hu, P. *Phys. Rev. Lett.* **2003**, *91*, 266102. (c) Liu, Z. P.; Jenkins, S. J.; King, D. A. *Phys. Rev. Lett.* **2005**, *94*, 196102.

(9) (a) Molina, L. M.; Hammer, B. *Phys. Rev. Lett.* **2003**, *90*, 206102. (b) Molina, L. M.; Hammer, B. *J. Chem. Phys.* **2005**, *123*, 161104. (c) Lopez, N.; Norskov, J. K. *J. Am. Chem. Soc.* **2002**, *124*, 11262. (d) Lopez, N.; Janssens, T. V. W.; Clausen, B. S.; Xu, Y.; Mavrikakis, M.; Bligaard, T.; Norskov, J. K. *J. Catal.* **2004**, *223*, 232.

(10) Sanchez, A.; Abbet, S.; Heiz, U.; Schneider, W. D.; Häkkinen, H.; Barnett, R. N.; Landman, U. *J. Phys. Chem. A* **1999**, *103*, 9573. (b) Yoon, B.; Hakkinen, H.; Landman, U.; Wirz, A. S.; Antonietti, J. M.; Abbet, S.; Judai, K.; Heiz, U. *Science* **2005**, *307*, 403. (c) Lee, S.; Fan, C.; Wu, T.; Anderson, S. L. *J. Am. Chem. Soc.* **2004**, *126*, 5682.

(11) Cho, A. *Science* **2003**, *299*, 1684.

(12) (a) Stolcic, D.; Fischer, M.; Gantefor, G.; Kim, Y. D.; Sun, Q.; Jena, P. *J. Am. Chem. Soc.* **2003**, *125*, 2848. (b) Sun, Q.; Jena, P.; Kim, Y. D.; Fischer, M.; Gantefor, G. *J. Chem. Phys.* **2004**, *120*, 6510. (c) Kimble, M. L.; Castleman, A. W., Jr.; Mitric, R.; Burgel, C.; Bonacic-Koutecky, V. *J. Am. Chem. Soc.* **2004**, *126*, 2526. (d) Hagen, J.; Socaciu, L. D.; Elijazyfer, M.; Heiz, U.; Bernhardt, T. M.; Woste, L. *Phys. Chem. Chem. Phys.* **2002**, *4*, 1707. (e) Socaciu, L. D.; Hagen, J.; Bernhardt, T. M.; Woste, L.; Heiz, U.; Häkkinen, H.; Landman, U. *J. Am. Chem. Soc.* **2003**, *125*, 10437.

(13) (a) Wallace, W. T.; Whetten, R. L. *J. Phys. Chem. B* **2000**, *104*, 10964. (b) Wallace, W. T.; Whetten, R. L. *J. Am. Chem. Soc.* **2002**, *124*, 7499. (c) Wallace, W. T.; Wyrwas, R. B.; Leavitt, A. J.; Whetten, R. L. *Phys. Chem. Chem. Phys.* **2005**, *7*, 930.

(14) (a) Nygren, M. A.; Siegbahn, P. E. M.; Jin, C.; Guo, T.; Smalley, R. E. *J. Chem. Phys.* **1991**, *95*, 6181. (b) Lee, T. H.; Ervin, K. M. *J. Phys. Chem.* **1994**, *98*, 10023. (c) Veldeman, N.; Lievens, P.; Andersson, M. *J. Phys. Chem. A* **2005**, *109*, 11793. (d) Balteanu, I.; Balaj, O. P.; Fox, B. S.; Beyer, M. K.; Bastl, Z.; Bondybey, V. E. *Phys. Chem. Chem. Phys.* **2003**, *5*, 1213.

(15) (a) Neumaier, M.; Weigend, F.; Hampe, O.; Kappes, M. M. *J. Chem. Phys.* **2005**, *122*, 104702. (b) Neumaier, M.; Weigend, F.; Hampe, O.; Kappes, M. M. *J. Chem. Phys.* **2006**, *125*, 104308.

(16) (a) Liang, B.; Andrews, L. *J. Phys. Chem. A* **2000**, *104*, 9156. (b) Jiang, L.; Xu, Q. *J. Phys. Chem. A* **2005**, *109*, 1026. (c) Xu, Q.; Jiang, L. *J. Phys. Chem. A* **2006**, *110*, 2655.

(17) (a) Fielicke, A.; von Helden, G.; Meijer, G.; Pedersen, D. B.; Simard, B.; Rayner, D. M. *J. Am. Chem. Soc.* **2005**, *127*, 8146. (b) Fielicke, A.; von Helden, G.; Meijer, G.; Simard, B.; Rayner, D. M. *J. Phys. Chem. B* **2005**, *109*, 23935. (c) Luttgens, G.; Pontius, N.; Bechthold, P. S.; Neeb, M.; Eberhardt, W. *Phys. Rev. Lett.* **2002**, *88*, 076102.

(18) (a) Häkkinen, H.; Landman, U. *J. Am. Chem. Soc.* **2001**, *123*, 9704. (b) Yoon, B.; Hakkinen, H.; Landman, U. *J. Phys. Chem. A* **2003**, *107*, 4066. (c) Wu, X.; Senapati, L.; Nayak, S. K.; Selloni, A.; Hajaligol, M. *J. Chem. Phys.* **2002**, *117*, 4010.

(19) (a) Varganov, S. A.; Olson, R. M.; Gordon, M. S.; Meitu, H. *J. Chem. Phys.* **2003**, *119*, 2531. (b) Varganov, S. A.; Olson, R. M.; Gordon, M. S.; Mills, G.; Meitu, H. *Chem. Phys. Lett.* **2003**, *368*, 778. (c) Mills, G.; Gordon, M. S.; Meitu, H. *Chem. Phys. Lett.* **2002**, *359*, 493.

(20) (a) Mitric, R.; Burgel, C.; Bonacic-Koutecky, V. *Proc. Natl. Acad. Sci. USA* **2007**, *104*, 10314. (b) Yuan, D. W.; Zeng, Z. *J. Chem. Phys.* **2004**, *120*, 6574. (c) Ding, X.; Li, Z.; Yang, J.; Hou, J. G.; Zhu, Q. *J. Chem. Phys.* **2004**, *120*, 9594.

(21) Zhai, H. J.; Wang, L. S. *J. Chem. Phys.* **2005**, *122*, 051101.

(22) Taylor, K. J.; Jin, C.; Conceicao, J.; Wang, L. S.; Cheshnovsky, O.; Johnson, B. R.; Norlander, P. J.; Smalley, R. E. *J. Chem. Phys.* **1990**, *93*, 7515.

(23) Zhai, H. J.; Kiran, B.; Dai, B.; Li, J.; Wang, L. S. *J. Am. Chem. Soc.* **2005**, *127*, 12098.

(24) (a) Imbihl, R.; Ertl, G. *Chem. Rev.* **1995**, *95*, 697. (b) Somorjai, G. A. *Nature* **2004**, *430*, 730.

(25) (a) Wang, L. S.; Cheng, H. S.; Fan, J. *J. Chem. Phys.* **1995**, *102*, 9480. (b) Wang, L. S.; Wu, H. *In Advances in Metal and Semiconductor Clusters. IV. Cluster Materials*; Duncan, M. A., Ed.; JAI Press: Greenwich, CT, 1998; pp 299−343.

(26) (a) Wang, L. S.; LiX. *In Clusters and Nanostructure Interfaces*; Jena, P.; Khanna, S. N.; Rao, B. K. Eds.;World Scientific: Englewood Cliffs, NJ, 2000; pp 293−300. (b) Akola, J.; Manninen, M.; Hakkinen, H.; Landman, U.; Li, X.; Wang, L. S. *Phys. Rev. B* **1999**, *60*, R11297. (c) Zhai, H. J.; Wang, L. S.; Alexandrova, A. N.; Boldyrev, A. I. *J. Chem. Phys.* **2002**, *117*, 7917.

(27) Bylaska, E. J., et al., *NWChem, A Computational Chemistry Package for Parallel Computers, Version 5.0*; Pacific Northwest National Laboratory: Richland, Washington 99352, USA, 2008.

(28) Hehre, W. J.; Ditchfield, R.; Pople, J. A. *J. Chem. Phys.* **1972**, *56*, 2257.

(29) Andrae, D.; Häusserman, U.; Dolg, M.; Stoll, H.; Preuss, H. *Theor. Chim. Acta* **1990**, *77*, 123.

(30) Martin, J. M. L.; Sundermann, A. *J. Chem. Phys.* **2001**, *114*, 3408.

(31) (a) Becke, A. D. *J. Chem. Phys.* **1993**, *98*, 1372–5648. (b) Lee, C.; Yang, W.; Parr, R. G. *Phys. Rev. B* **1988**, *37*, 785. (c) Stephens, P. J.; Devlin, F. J.; Chabalowski, C. F.; Frisch, M. J. *J. Phys. Chem.* **1994**, *98*, 11623. (d) Stephens, P. J.; Devlin, F. J.; Ashvar, C. S.; Chabalowski, C F.; Frisch, M. J. *Faraday Discuss* **1994**, *99*, 103.

(32) Tozer, D. J.; Handy, N. C. *J. Chem. Phys.* **1998**, *109*, 10180.
(33) Pyykkö, P. *Angew. Chem. Int. Ed* **2004**, *43*, 4412.
(34) (a) Parks, E. K.; Kerns, K. P.; Riley, S. J. *J. Chem. Phys.* **2000**, *112*, 3384. (b) Kerns, K. P.; Parks, E. K.; Riley, S. J. *J. Chem. Phys.* **2000**, *112*, 3394.
(35) (a) Manard, M. J.; Kemper, P. R.; Bowers, M. T. *J. Am. Chem. Soc.* **2005**, *127*, 9994. (b) Manard, M. J.; Kemper, P. R.; Bowers, M. T. *Int. J. Mass Spectrom.* **2006**, *249*, 252.
(36) The calculation details about these values can be found in ref 23. The basis sets used there are different from the current work. The calculated energy difference from the two kinds of basis sets is 0.03−0.05 eV for the same system.
(37) Li, J.; Li, X.; Zhai, H. J.; Wang, L. S. *Science* **2003**, *299*, 864.
(38) The bonding analysis calculations were performed using PW91 exchange−correlation functional and the zero-order regular approximation implemented in ADF 2006.01 SCM, Theoretical Chemistry, Vrije Universiteit, Amsterdam, The Netherlands (http://www.scm.com). (a) Perdew, J. P.; Wang, Y. *Phys. Rev. B* **1992**, *45*, 13244. (b) van Lenthe, E.; Baerends, E. J.; Snijders, J. G. *J. Chem. Phys.* **1993**, *99*, 4597.

JP803161B